Adam J. Moulé, Henry J. Snaith, Markus Kaiser, Heike Klesper, David M. Huang, Michael Grätzel, and Klaus Meerholz

Optical description of solid-state dye-sensitized solar cells. I. Measurement of layer optical properties

Journal of Applied Physics, 2009; 106(7):073111-1-073111-9

Optical description of solid-state dye-sensitized solar cells. I. Measurement of layer optical properties

Cite as: J. Appl. Phys. **106**, 073111 (2009); https://doi.org/10.1063/1.3204982
Submitted: 12 May 2009 . Accepted: 10 July 2009 . Published Online: 14 October 2009

Adam J. Moulé, Henry J. Snaith, Markus Kaiser, Heike Klesper, David M. Huang, Michael Grätzel, and Klaus Meerholz

Optical description of solid-state dye-sensitized solar cells. I. Measurement of layer optical properties

Adam J. Moulé,[1,2] Henry J. Snaith,[3] Markus Kaiser,[2] Heike Klesper,[2] David M. Huang,[1] Michael Grätzel,[4] and Klaus Meerholz[2,a)]
[1]*Chemical Engineering and Materials Science, University of California, Davis, California 95616, USA*
[2]*Physikalische Chemie, Universität Köln, Luxemburgerstr. 116, 50939 Köln, Germany*
[3]*Clarendon Laboratory, Department of Physics, University of Oxford, Parks Road, Oxford OX1 3PU, United Kingdom*
[4]*Institut des Sciences et Ingenierie Chimique, École Polytechnique Fédérale de Lausanne, CH-1015 Lausanne, Switzerland*

(Received 12 May 2009; accepted 10 July 2009; published online 14 October 2009)

The efficiency of a photovoltaic device is limited by the portion of solar energy that can be captured. We discuss how to measure the optical properties of the various layers in solid-state dye-sensitized solar cells (SDSC). We use spectroscopic ellipsometry to determine the complex refractive index of each of the various layers in a SDSC. Each of the ellipsometry fits is used to calculate a transmission spectrum that is compared to a measured transmission spectrum. The complexities of pore filling on the fitting of the ellipsometric data are discussed. Scanning electron microscopy and energy dispersive x-ray spectroscopy is shown to be an effective method for determining pore filling in SDSC layers. Accurate effective medium optical constants for each layer are presented and the material limits under which these optical constants can be used are discussed. © *2009 American Institute of Physics*. [doi:10.1063/1.3204982]

I. INTRODUCTION

Dye-sensitized solar cells (DSCs) offer a low-cost alternative to traditional crystalline photovoltaic devices.[1] The cost reduction comes from reduced material costs and reduced preparation costs, i.e., lower cost equipment and lower temperature production. The high efficiency of liquid DSCs (>11%) (Ref. 2) derives not from impressive electrical features of an individual material but from judicious molecular design and control of nanoarchitecture. The standard DSC is based on a mesoporous TiO_2 layer covered with a monolayer of sensitizing dye molecules and filled with a redox-active electrolyte (iodide/tri-iodide based).[1] The dye molecules absorb light and transfer an electron to the TiO_2 upon photoexcitation. The redox electrolyte quenches the oxidized dye molecule and carries the "hole" to the anode. Recent research attention has been focused on replacing the electrolyte with solid-state hole conductors because there are concerns that the electrolyte will, over long time periods, leak out of the liquid cell or degrade.[3] A recent efficiency record for solid-state DSCs (SDSCs) of 5.1% was shown for hole conductors based on 2,2′,7,7′-tetrakis(*N*, *N*-di-*p*-methoxyphenylamine)-9,9′-spirobifluorene (spiro-MeOTAD).[4]

One major difference between the solid-state and liquid DSCs is that the external quantum efficiency (EQE) is a limiting factor in the solid-state devices. While the thickness of a liquid DSC has been optimized to 13–30 μm,[5,6] the highest efficiency solid-state devices are only ~2 μm.[7] The maximum thickness is limited in part by the ability of the organic hole conductor to penetrate into the mesoporous TiO_2.[8,9] The record 5.1% efficiency device showed an EQE maximum of 60% near the absorbance maximum and reduced EQE throughout the rest of the spectrum. Though the electrical function of the SDSC has been studied using a variety of methods,[10–12] it is not clear to what extent the EQE is limited by light absorbance and what percentage of the absorbed light is eventually lost through other channels.

In this and the subsequent article (Parts I and II, respectively), we report on the measurement of the complex refractive index of the various layers in a SDSC and optical modeling of completed devices. In Part I, we focus on accurately determining the complex refractive index $[n(\lambda)+ik(\lambda)]$ of each of the device layers. $n(\lambda)+ik(\lambda)$ is determined using spectroscopic ellipsometry in reflection mode and verified using UV/vis spectroscopy in transmission mode. However, since the nanostructured layers contain complex mixtures of materials that are sensitive to fabrication conditions, considerable discussion is required to define the conditions under which the optical model is valid. In addition, scanning electron microscopy (SEM) and energy dispersive x-ray (EDX) spectroscopy are used to determine the extent to which the pores of the mesoporous TiO_2 layer are filled with the spiro-MeOTAD. In Part II, an optical model of photoabsorbance in a completed device is developed. We use our calculation of the absorbed light in comparison with EQE measurements to determine the internal QE or electrical efficiency in the active layer of a SDSC. The implications for improved device efficiency are discussed in Part II.[13]

II. EXPERIMENTAL

Ellipsometric data were obtained using a variable angle spectroscopic ellipsometer (VASE) in the wavelength range of 369–1001 nm (3.36–1.23 eV) in steps of 10 nm. The ellipsometric data was taken in nulling mode and averaged

a)Electronic mail: klaus.meerholz@uni-koeln.de.

over four quadrants to reduce systematic errors. Data was taken at the average of the Brewster angles for 400, 550, and 850 nm light. The data was fit to a single angle of incidence (AOI) for each sample. The layer thickness of the sample was measured independently using a Dektak 3 surface profiler and SEM to reduce the errors resulting from the correlation of layer thickness and refractive index. The measured thickness was used as the starting thickness for fitting of the ellipsometric data and as thickness for transmission data. The fitted sample thickness was not allowed to vary more than 3 nm from the measured thickness. Only reflection ellipsometry was performed in this study. The samples were stored in the dark until measured. Each sample was measured at several locations and at several angles for verification purposes, though presented data is for a single measurement at a single AOI. Ellipsometry was performed on a Nanofilm EP3 ellipsometer and transmission measurements were performed using a Varian Cary UV/Vis spectrophotometer.

Ellipsometry cannot effectively be practiced on completed devices. All ellipsometry samples were prepared on Si/SiO_2 substrates with a thick (~300 nm) SiO_2 layer (optical properties[14,15]). Samples were fabricated on fused silica substrates under the same conditions for transmission measurements. The compact TiO_2 layer was coated to a thickness of 40–100 nm by aerosol spray pyrolysis deposition at 450 °C using oxygen as the carrier gas.[16,17] Mesoporous TiO_2 layers were doctor bladed onto the substrate from a homemade TiO_2 nanoparticle paste[18] to give dry film thicknesses between 1.4 and 2 μm, governed by the height of the doctor blade. These films were then slowly heated to 500 °C (ramped over 30 min) and baked at this temperature for 30 min under an oxygen flow. The final sintered film porosity was 0.6 as determined by nitrogen absorption. Prior to dye deposition, the nanoporous films were soaked in a 0.02 M aqueous solution of $TiCl_4$ for 6 h at room temperature in the dark. After rinsing with de-ionized water and drying in air, the films were baked once more at 500 °C for 45 min under oxygen flow with subsequent cooling to 70 °C and placed in a dye solution overnight. Two sensitizer dyes were used in this study. Z907 is a ruthenium-based dye with a thiocyanate bipyridyl complex and hydrophobic side chains.[19] D149 is an indoline-based push-pull organic sensitizer with an exceptionally high extinction coefficient of 68,000 cm^{-1} M^{-1}.[20] The dye solutions comprised 0.5 mM of Z907 or 0.2 mM of D149 in acetonitrile and tert-butyl alcohol (volume ratio 1:1). The hole-transporting material used was spiro-MeOTAD, which was dissolved in chlorobenzene at a typical concentration of 180 mg ml^{-1}. After fully dissolving the spiro-MeOTAD at 100 °C for 30 min, the solution was cooled and tert-butyl pyridine (tbp) was added directly to the solution with a volume-to-mass ratio of 1:26 μl mg^{-1} tbp:spiro-MeOTAD. Lithium bis(trifluoromethylsulfonyl)imide salt (Li-TFSI) ionic dopant was predissolved in acetonitrile at 170 mg ml^{-1}, then added to the hole-transporter solution at 1:12 μl mg^{-1} of Li-TFSI solution:spiro-MeOTAD. We note that no chemical oxidant was used in the hole transporter.[21] The dye-coated mesoporous films were briefly rinsed in acetonitrile and dried in air for 1 min. A small quantity (20–70 μl) of the spiro-MeOTAD solution was dispensed onto each dye-coated substrate and left for 40 s before spin coating at 2000 rpm for 25 s in air. Spiro-MeOTAD layers were also spin coated directly onto the substrates from the same solution.

SEM and EDX analysis were performed on a Zeiss Supra 40 VP microscope with a thermic field effect emitter and an Oxford Inca Drycool EDX detector. The samples that were measured using EDX were first coated with 80 nm of Pt by sputtering and then broken. The broken edge was polished using a Jeol SM-09010 cross-section polisher.[22] The sputtered Pt layer was added to maintain the structure of the soft spiro-MeOTAD layer.

III. RESULTS AND DISCUSSION

A. Ellipsometry of a single interface

Spectroscopic ellipsometry is an extremely powerful method to investigate the optical properties of complex and multilayer thin-film samples. For a substrate, the ellipsometric variables (Δ and Ψ) can be used to calculate the complex refractive index ($n+ik$) exactly.[23] Typically, however, one is interested in the optical properties of one or more films deposited on top of a well defined substrate. In this case, even if the substrate's optical properties are known, the addition of the layer with thickness (d) increases the number of unknown variables and so the refractive index must be iteratively fit using data from multiple-angle and/or multiple-wavelength measurements. VASE has emerged as a powerful tool for determining the $n(\lambda)+ik(\lambda)$ but the fitting procedure must be carefully applied to avoid the addition of excess variables, which can lead to multiple fit minima and incorrect assignment of the optical properties. Quantitatively, the Δ and Ψ spectral data are fit by minimizing the mean squared error (MSE).[23] We follow the procedure and minimize the MSE as outlined by Persson *et al.*[24]

A SDSC is composed of a number of layers [Fig. 1(a)]. The incident sunlight enters through a soda lime glass substrate and passes to a transparent fluorine-doped tin oxide layer, followed by compact TiO_2, then porous TiO_2 nanoparticles covered with dye molecules and with the pores filled with spiro-MeOTAD, next is pure spiro-MeOTAD, and finally the metal back electrode composed of either Au or Ag. Clearly, it is not possible to measure or fit all of the device thicknesses or optical properties simultaneously. Therefore, the optical properties of each of the device layers are determined separately from specially prepared samples and then used in an optical model to determine the net effect of the entire layer stack. The process for measuring each of the layers separately will now be addressed.

As stated above, $n+ik$ can be determined exactly using a single measurement for an optically thick substrate sample. We used this to determine n and k for Au and Ag, the metal electrode materials, at each wavelength separately for an average MSE of ≤ 0.1 for each measurement. This measurement error comes from machine errors in correctly determining the exact polarization of the reflected radiation. Figure 2 (top) shows the measured $n(\lambda)$ and $k(\lambda)$ spectra and a comparison with literature data.[25] Clearly the measured and literature data are very close but not identical. This is because

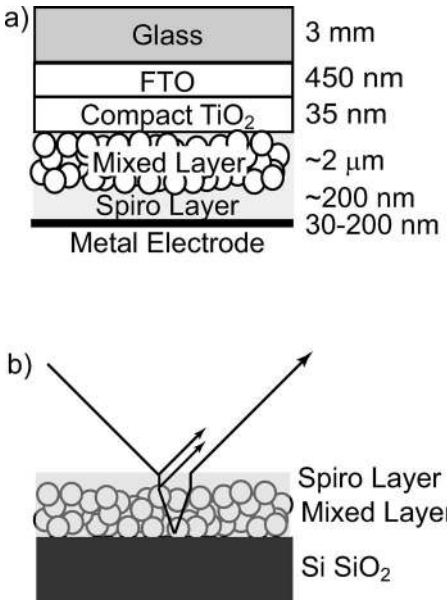

FIG. 1. (a) Schematic diagram showing the various layers and estimated thicknesses of the layers in a SDSC. (b) Reflection ellipsometry measurement setup for SDSCs. The complex refractive index cannot be measured for the mixed layer for wavelengths at which the spiro-MeOTAD layer absorbs strongly due to a filtering effect.

the measured samples were prepared by evaporating ~200 nm of metal onto a quartz substrate, which yields a surface with a variety of domain orientations. The literature values were measured for a single crystalline (001) surfaces in each case. Our measured $n(\lambda)$ and $k(\lambda)$ spectra are therefore more accurate representatives of the real optical properties that exist in the DSCs we want to model. Also displayed in Fig. 2 (middle) and (bottom) respectively, are the reflectivity (R) and dissipation (D) spectra assuming an air/metal interface where

$$R = \frac{(n_t - n_i)^2 + (k_t - k_i)^2}{(n_t + n_i)^2 + (k_t + k_i)^2} \tag{1}$$

and

$$D = 1 - R. \tag{2}$$

The indices i and t represent incident and transmitted in the two materials, which are in this case air and a metal surface.

The reflectivity of the Ag surface is clearly higher across the entire spectrum than the Au surface or even the AuAg surface. This higher reflectivity has been shown to increase the light absorbance in the active layer of SDSCs and to increase the short circuit-current density (J_{sc}) by over 20% for a record power conversion efficiency of 5.1%.[4]

B. Optical properties of individual layers

Individual layers of compact TiO_2 and spiro-MeOTAD were prepared as stated in the experimental section. The Δ and Ψ spectra for the compact TiO_2 were measured using an incidence angle of 59.8°, which was determined using the average Brewster angles for this sample at 400, 550, and 800 nm. The spectra were taken over all four measurement quadrants and then averaged. Next an optical model of the

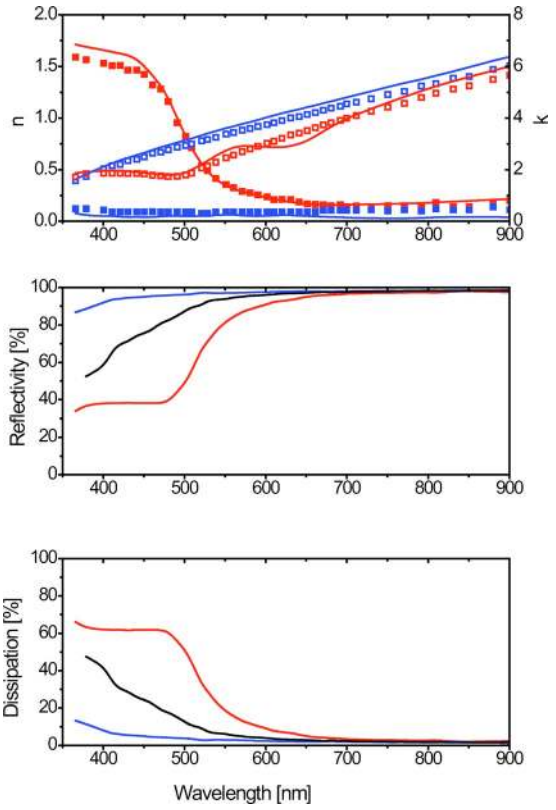

FIG. 2. (Color online) Top: Wavelength dependence of $n(\lambda)$ (■, left axis) and $k(\lambda)$ (□, right axis) of vacuum-deposited Au (red) and Ag (blue). The lines are n and k taken from literature of single crystal surfaces. Middle: Calculated reflectivity from Au (red), Ag (blue), and 5 nm Au on 200 nm Ag (black) substrates in air. Bottom: Calculated dissipation of light into Au (red), Ag (blue), and 5 nm Au on 200 nm Ag (black) substrates in air. All calculations assume an optically thick metal layer.

compact TiO_2 layer was developed using a Cauchy function, which is often used to approximate the complex refractive index below the band gap of a material, and a Lorentzian oscillator. A Cauchy function has the form

$$n(\lambda) = A_n + B_n\lambda^{-2} + C_n\lambda^{-4}, \tag{3}$$

where A_n represents the expected value of n as λ approaches ∞. For fitting the $n(\lambda)$ of both spiro-MeOTAD and TiO_2, C_n was set to zero, leaving two fit parameters. Each of these layers is composed of an amorphous material that contains local deep traps and scattering sites that would not be found in a crystalline sample. To account for the reduced transmittance throughout the spectrum, including below the optical band gap, a constant minimum k value is included in the model and reported in Table I as k_{min}.

A Lorentzian oscillator has the general form

$$2nk = \frac{IE_0\Gamma E}{(E^2 - E_0^2)^2 + \Gamma^2 E^2}, \tag{4}$$

where E_0 is the peak center energy, I represents the intensity of the peak, and Γ is the full width at half maximum. The real and imaginary components of the Lorenzian oscillator are separated using the Kramers Kronig relations and added to the Cauchy function for fitting. The fit parameters for the Cauchy and Lorentzian oscillator functions are listed in Table I. Finally, the compact TiO_2 layer has a thickness (d).

TABLE I. Model parameters used for the ellipsometric fits to SDSC layers.

	Cauchy parameters			Harmonic oscillator			Anharmonic Bruggeman		
Layer	A_n	$B_n(\lambda^2)$	$k_{\min}$ E_0 (eV)	E_0	I (eV)	Γ (eV)	E_1 (eV)	v_2	MSE
TiO_2-comp	2.133	27818	0	3.916	10.9	0.091	⋯	⋯	3.87
spiro-MeOTAD	1.575	17900	0.0034	3.307	1.848	0.019	⋯	⋯	4.54
mixed	⋯	⋯	⋯	⋯	⋯	⋯	⋯	0.623	9.0
mixed-D149	⋯	⋯	⋯	2.317	0.617	0.454	1.096	0.637	14.44
mixed-Z907	⋯	⋯	⋯	2.473	0.095	0.450	0.958	0.688	21.71

So the fit to the compact TiO_2 layer was performed with six variables and yielded a MSE of 3.87. Figure 3 (top) shows the fitted $n(\lambda)$ and $k(\lambda)$ spectra for the compact TiO_2 layer.

The best fit to the measured ellipsometry parameters (Δ and Ψ) is determined by minimizing the MSE. However, for a multivariable fit, the parameter space can have multiple minima. It is, therefore, necessary to check whether the best fit $n(\lambda)$ and $k(\lambda)$ is in fact correct. To perform this check, we deposited compact TiO_2 layers onto quartz substrates and measured the absorbance spectra of these samples. Absorbance values for the whole sample were then calculated using the best fits $n(\lambda)$ and $k(\lambda)$ for TiO_2 and literature optical values for quartz. The absorbance (Abs) spectrum is calculated by relation to the transmission (T) by

$$\text{Abs} = -\log(T) \tag{5}$$

and T is

$$T = 1 - R - \sum_{i=1}^{m} D_m, \tag{6}$$

where D_m represents *dissipation* in each of the various layers m. Calculation of R, T, and D_m is detailed in other articles[26–28] and books[29] on optics. Figure 3 (bottom) shows a comparison of the measured UV/vis absorbance spectrum (solid line) and the calculated spectrum (dotted points) for two different TiO_2 layers on quartz substrates. In both cases, the best fit $n(\lambda)$ and $k(\lambda)$ are able to calculate the absorbance spectra exactly for wavelengths longer than 400 nm, indicating that the best fit data accurately represents the complex refractive index of the compact TiO_2 layer.

The spiro-MeOTAD layer was also prepared on a $Si-SiO_2$ substrate independently of the rest of the layers in a SDSC by spin coating. This sample was measured using spectroscopic ellipsometry following the same method as the compact TiO_2 layer. The measurement angle that best matched the average Brewster angle for the sample across the entire spectrum was 60°. These data were again fit using the sample thickness, a Cauchy function, and a Lorentzian oscillator. The fit parameters for the Cauchy and Lorentzian oscillator functions and the MSE are listed in Table I. The corresponding best fit $n(\lambda)$ and $k(\lambda)$ are displayed in Fig. 4 (top).

Again it is necessary to verify that the best fit $n(\lambda)$ and $k(\lambda)$ can be used to accurately calculate an absorbance spectrum. Figure 4 (bottom) also shows an absorbance spectrum for a 536-nm-thick spiro-MeOTAD layer deposited onto a quartz substrate. The "waviness" in the transparent part of the spectrum comes from optical interference in the layer. The transparent part of the spectrum is displayed as an inset to show that all of the interference fringes are captured in the

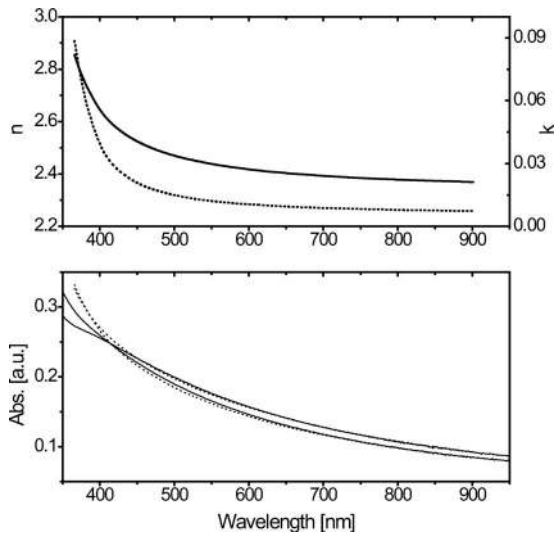

FIG. 3. Top: Best fit refractive index (solid line) and extinction coefficent (dotted line) vs wavelength from ellipsometry measurements of compact TiO_2 layers on $Si-SiO_2$ substrates. Bottom: UV/vis spectra of compact TiO_2 layers on quartz with thicknesses of 34 and 37 nm (solid lines). Included are the calculated absorbances for the 34 and 37 nm (dotted lines) using the best fit n and k.

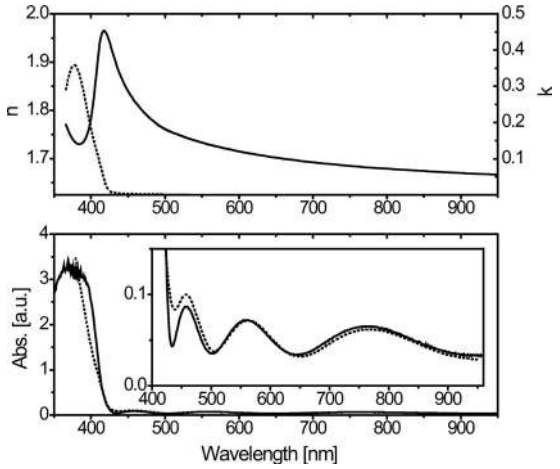

FIG. 4. Top: Best fit refractive index (solid line) and extinction coefficent (dotted line) vs wavelength from ellipsometry measurements. Bottom: Measured UV/vis absorbance spectrum for a 536 nm spiro-MeOTAD layer on a quartz substrate (line) and the calculated absorption (dotted) assuming the same thickness and the $n(\lambda)+ik(\lambda)$ from ellipsometry. Inset: A blowup of the absorbance data in the transparent region of the spectrum

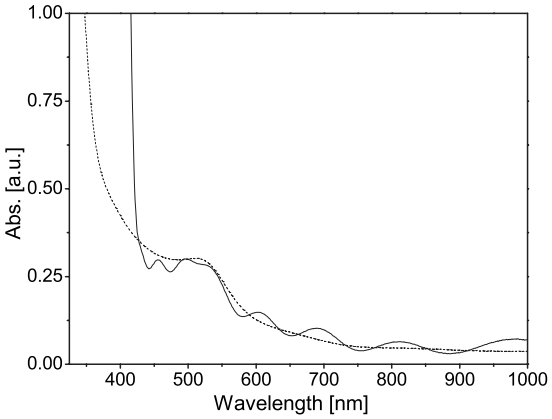

FIG. 5. UV/vis spectra of an approximately 940-nm-thick, mesoporous TiO_2 layer that has been covered with a monolayer of Z907 dye and mounted onto a quartz substrate (dotted line). UV/vis spectrum of an identical dye-covered mesoporous film that has also been filled with spiro-MeOTAD (solid line).

calculated absorbance from the best fit $n(\lambda)$ and $k(\lambda)$. The fit to the UV/vis spectrum is excellent everywhere in the spectrum except between 420 and 480 nm, where the best fit data slightly overestimates the actual absorbance and in the UV, where an absorbance of over 3 cannot be accurately measured by the spectrometer. Also notice that the onset of absorbance at 420 nm is very steep. The very strong absorbance of the spiro-MeOTAD places a limit on the wavelength range that can be fit. So much of the incident probe light is absorbed at shorter wavelengths that the $n(\lambda)$ and $k(\lambda)$ were fit for individual wavelengths using a multiangle data aquisition with the assumption that the spiro-MeOTAD layer is optically thick.

C. Optical properties of mixed multilayers

As has been shown above, the $n(\lambda)$ and $k(\lambda)$ spectra for the metal, compact TiO_2, and spiro-MeOTAD layers can be fit individually. The active layer of a SDSC is a porous layer of TiO_2 nanoparticles covered in a monolayer of dye molecules and then filled with spiro-MeOTAD. We first attempted to determine the optical properties of the unfilled porous TiO_2 layer. This proved to be impossible because (1) the surface of the porous TiO_2 film was very rough (rms roughness >25 nm determined using atomic force microscopy (AFM) and (2) the mesoporous film itself scattered light. This combination of scattering at the interface and scattering within the film made accurate ellipsometry impossible. However, when a thin porous TiO_2 film was filled with spiro-MeOTAD, scattering was reduced and ellipsometry was again possible.

Figure 5 shows UV/vis spectra of porous TiO_2 layers that have a monolayer of Z907 dye have been prepared on quartz substrates. The layers either have (solid line) or have not (dotted line) been filled with spiro-MeOTAD. In the filled porous layer, the interference pattern is clear throughout the spectrum, while in the unfilled porous layer, no interference pattern is present. This data shows that scattering dominates the optical effects in the unfilled porous film, while the filled porous film shows a clear and strong interference pattern, which makes it a good sample for ellipsometric analysis. A second observation is the strong absorbance beginning at 420 nm in the filled porous film. This strong absorbance is due to the spiro-MeOTAD (Fig. 4).

Next we measured and fit the $n(\lambda)$ and $k(\lambda)$ spectra for a porous layer of TiO_2 filled with spiro-MeOTAD. This sample was also prepared on a $Si-SiO_2$ substrate. The sample geometry in Fig. 1 (bottom) shows how the data was taken. The incident light must pass through a pure spiro-MeOTAD layer before reaching the mixed layer and then pass through the pure spiro-MeOTAD layer again before reaching the detector. Since the data acquired in an ellipsometry measurement is a change in light polarization, not light intensity, the sample fitting is very sensitive to whether the signal comes from light that has passed through the entire sample or has only reflected off the top surface. Beginning with the strong absorbance at 420 nm, the main reflected signal and polarization change come from the top surface rather than the mixed layer, which means that $n(\lambda)$ and $k(\lambda)$ cannot accurately be measured for the mixed porous layer for wavelengths shorter than 420 nm. The data shown for these wavelengths therefore have uncertainties that are unacceptable for optical device modeling.

This sample was measured using spectroscopic ellipsometry following the same method as the compact TiO_2 layer. The measurement angles between 65° and 70° were the best match to the Brewster angle across the entire spectrum. The data was fit to a four-layer model, from bottom to top $Si-SiO_2$—mixed layer—spiro-MeOTAD. Since the substrate and spiro-MeOTAD layers had already been fit independently, only the mixed layer parameters and thicknesses had to be considered for this sample. The mixed layer was fit by combining the dielectric constants of the compact TiO_2 and spiro-MeOTAD using the Bruggeman effective medium approximation[30]

$$\varepsilon_{\text{eff}} = \varepsilon_2 \frac{3\varepsilon_1 + 2\upsilon_2(\varepsilon_2 - \varepsilon_1)}{3\varepsilon_2 - 2\upsilon_2(\varepsilon_2 - \varepsilon_1)}, \tag{7}$$

where ε_{eff} is the effective permittivity of a homogeneous medium, ε_2 is the permittivity of particles dispersed in a medium with ε_1, and υ_2 is the volume fraction of the dispersed component. This model allows a two-phase mixture of a complex dielectric medium to be modeled as a dilute phase of spheres in a host medium. This approximation has been shown to be accurate as long as the host and dilute phases are correctly assigned.[30] Interestingly, in studies of soil in water, it was experimentally shown that the dilute phase can have volume fractions higher than the host medium and still provide an accurate representation of the mixed permittivity.[30] For fitting of the mixed layer ellipsometric data, the host was the TiO_2 matrix and the dilute spheres spiro-MeOTAD. The fit used the measured data for compact TiO_2 as presented in Fig. 3 and for spiro-MeOTAD as presented in Fig. 4. The only three fit parameters were therefore the two layer thicknesses and υ_2. For the mixed layer, the measured Δ and Ψ data were fit independently between $\lambda = 420$ and 950 nm at an AOI of 65° and 70° Fig. 6 (top). The layer thickness was held constant for each AOI and a υ_2 of 0.623 ± 0.01 was found. The resulting $n(\lambda)$ and

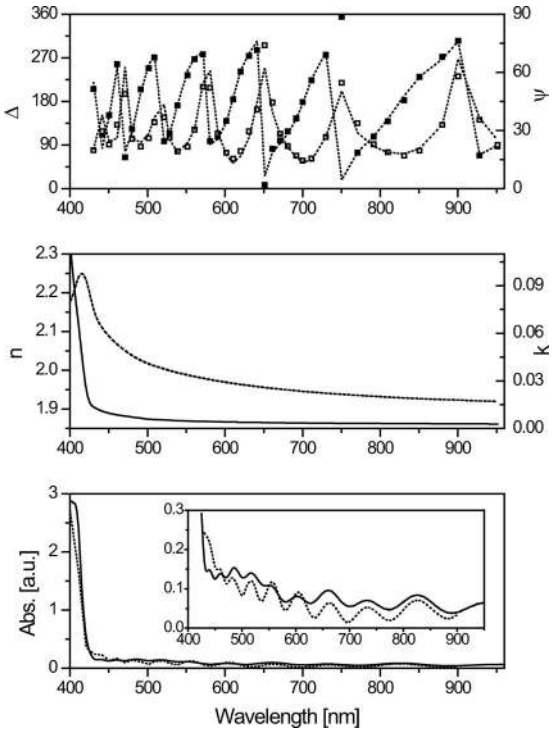

FIG. 6. Best fit for optical properties for a porous TiO_2 layer filled with spiro-MeOTAD (764 nm) and covered with a pure spiro-MeOTAD layer (306 nm). Top: Measured △ (■, left axis) and Ψ (□, right axis) with the best fit to the measured data displayed (dotted lines). Middle: Refractive index (solid line, left) and extinction coefficient (dotted line, right). Bottom: UV/vis spectrum of a 1340 nm mixed layer with a 320 nm layer of spiro-MeOTAD covering the surface on a quartz substrate (solid line) and the calculated absorbance (dotted line) assuming a three-layer (quartz—mixed layer—spiro-MeOTAD). The measured thicknesses are taken from profilometry and the $n(\lambda)+ik(\lambda)$ from ellipsometry. The inset shows a blowup of the absorbance data in the transparent region of the spectrum.

$k(\lambda)$ are in Fig. 6 (middle). A fit comparison to an absorptivity spectrum of a porous TiO_2 layer filled with spiro-MeOTAD is shown in Fig. 6 (bottom).

The calculated spectrum fits remarkably well to the measured absorbance spectrum but the calculated spectrum has a larger difference between maxima and minima in the interference fringes below the band gap. This difference arises because the top surface of the TiO_2 layer is not perfectly flat and has a peak-to-peak roughness (measured using AFM) of over 70 nm. In a fit of optical constants using ellipsometry, a roughness layer is typically modeled as a weighted average of the two layers involved, in this case the mixed and spiro-MeOTAD layers. We accounted for the roughness layer by fitting it to two mixed layers with different mixing ratios of spiro-MeOTAD to TiO_2. Each of these layers required two variables, a thickness and v_2. Since the proportion of spiro-OMeTAD can be expected to increase in the mixed roughness layer, using a Bruggeman approximation for both layers is acceptable. The addition of an extra layer did little to improve the fit to the measured Δ and Ψ spectral data. The MSE of the fit using one layer was 9 and the MSE assuming both mixed and mixed roughness layers was 8.7. In addition, identical improvement in MSE could be found for a wide variety of mixed roughness layer thicknesses. Since the addition of the mixed roughness layer did little to improve the fit but added considerably to the complexity of the fit (doubling the number of independent variables), the mixed layer is represented and modeled as a single layer for the rest of this article.

Finally, the $n(\lambda)$ and $k(\lambda)$ were measured and fit for porous TiO_2 layers that had been covered with a monolayer of dye and then filled with spiro-MeOTAD. We investigated two dyes. The organic D149 dye[5] and the ruthenium-based Z907 dye[7,8] have both been used in high-efficiency SDSC devices. In both cases, the $n(\lambda)$ and $k(\lambda)$ were measured using the same technique and using the same experimental considerations as the mixed layer described above. In order to get a good measurement, the dye-covered TiO_2 layer filled with spiro-MeOTAD had to be 900 nm thick or less to ensure that the pores were sufficiently filled. As for the mixed layer, the average Brewster angle was between 65° and 70°. However, due to the additional intensity losses that occur with light absorbance in the dyes, the reflected light intensity was higher for reflection off the air—spiro-MeOTAD and spiro-MeOTAD—mixed layers than for light that had passed through all of the layers for wavelengths <650 nm near the Brewster angle. For this reason, ellipsometric measurements of these layers were performed at 55° to 60°. While changing to a less glancing angle allows consistent measurements to be made, it also reduces the accuracy to which the thickness of the layer can be fit. The tradeoff was, in this case, necessary and appropriate.

In each case, the dye itself was fit by adding a single oscillator to the mixed-layer optical model. The D149 dye was represented by an asymmetric oscillator with values listed in Table I. The asymmetric oscillator model was developed for fitting the dielectric functions of amorphous materials, explicitly excludes intraband transitions,[31] and has the form

$$\phi(E) = \frac{IE_0\Gamma(E-E_1)^2}{(E^2-E_0^2)^2+\Gamma^2E^2}\frac{1}{E}, \quad E \geq E_1,$$

$$2nk(E) = 0, \quad E < E_1, \tag{8}$$

where I is the intensity, E_0 is the absorbance maximum, E_1 is the absorbance onset, and Γ is the peak width. The MSE of the fit to the mixed-D149 sample was 14.44 over the wavelength range of 420–950 nm. The high value of the MSE is partially due to the uncertainty of the layer thickness of the ellipsometry sample as described above. The $n(\lambda)$ and $k(\lambda)$ for the D149-mixed layer are shown in Fig. 7 (middle). As for all of the other layers, the quality of the fit was tested by comparing a UV/vis spectrum of the layer on quartz to a calculated spectrum [Fig. 7 (bottom)]. The sample in this case was quartz—D149-mixed layer—spiro-MeOTAD. The fit to the absorbance spectrum is good. All of the interference fringes are represented and the height of the absorbance peak is also accurate.

The Z907 dye was also represented by an asymmetric oscillator[31] with values listed in Table I. The MSE of the fit for this layer was 21.71 over the range of 420– 950 nm. The high value of the MSE is partially due to the uncertainty of the layer thickness of the ellipsometry sample as described above and higher than in the D149 samples because of the

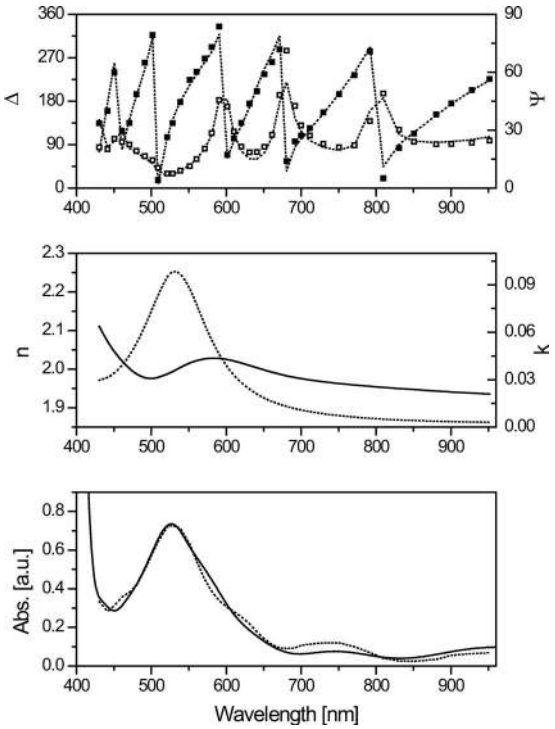

FIG. 7. Best fit for optical properties for a porous TiO_2 layer covered with D149 dye and filled with spiro-MeOTAD (607 nm) and covered with a pure spiro-MeOTAD layer (302 nm). Top: Measured △ (■, left axis) and Ψ (□, right axis) with the best fit to the measured data displayed (dotted lines). Middle: Refractive index (solid line, left) and extinction coefficient (dotted line, right). Bottom: UV/vis spectrum of a 302 nm mixed layer with a 187 nm layer of spiro-MeOTAD covering the surface on a quartz substrate (solid line) and the calculated absorbance (dotted line) assuming a three-layer (quartz—mixed layer—spiro-MeOTAD). The measured thicknesses are taken from profilometry and the $n(\lambda)+ik(\lambda)$ from ellipsometry. The inset shows a blowup of the absorbance data in the transparent region of the spectrum.

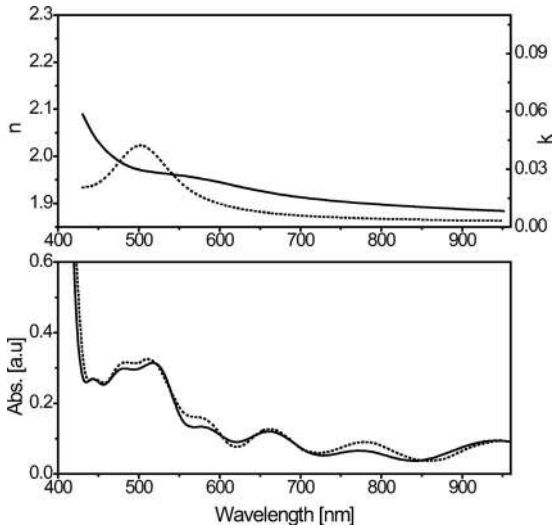

FIG. 8. Best fit for optical properties for a porous TiO_2 layer covered with Z907 dye and filled with spiro-MeOTAD (940 nm) and covered with a pure spiro-MeOTAD layer (524 nm). Top: Refractive index (solid line, left axis) and extinction coefficient (dotted line, right axis). Bottom: UV/vis spectrum (solid line) of a 564 nm mixed layer with a 610 nm layer of spiro-MeOTAD covering the surface on a quartz substrate (solid line) and the calculated absorbance (dotted line) assuming a three layer (quartz—mixed layer—spiro-MeOTAD layer). The measured thicknesses are taken from profilometry and the $n(\lambda)+ik(\lambda)$ from ellipsometry. The inset shows a blowup of the absorbance data in the transparent region of the spectrum.

larger layer thickness, which likely includes more voids in the pore structure. The $n(\lambda)$ and $k(\lambda)$ for the Z907-mixed layer are shown in Fig. 8 (top). As for all of the other layers, the quality of the fit was tested by comparing a UV/vis spectrum of the layer on quartz to a calculated spectrum. The sample in this case is quartz—Z907-mixed layer—spiro-MeOTAD. The fit to the absorbance spectrum is good. All of the interference fringes are represented and the height of the absorbance peak is also accurate.

Comparison of the $n(\lambda)$ and $k(\lambda)$ for the two dye-covered mixed layer yields some interesting insights into the differences between the two dyes. First, the D149 dye has a redshifted absorbance maximum of ~530 nm with respect to the ~500 nm absorbance maximum of the Z907 dye. The D149 dye also has a much higher $k(\lambda)$ than the Z907 dye near the absorbance maximum. The higher $k(\lambda)$ of the D149 dye leads to a much higher absorbance in a 302 nm mixed layer than is seen in the 564 nm layer covered with the Z907 dye. Interestingly, the higher absorbance of the D149 dye also has a strong effect on the $n(\lambda)$ of the mixed layer, where the $n(\lambda)$ of the Z907-mixed layer varies little from the dye-free mixed layer.

Another interesting question is whether the addition of dye to the TiO_2 surface changes the ability of spiro-MeOTAD to penetrate into the mesoporous TiO_2. The answer is inconclusive. As estimated from ellipsometry, the mixed layers with no dye and with D149 had (see Eq. (7)) spiro-MeOTAD volume fractions (υ_2) of 0.623 and 0.637 for mixed layer thicknesses of 764 and 302 nm, respectively, which shows that the mixing ratios are identical within experimental error for thin layers. The mixed layer with Z907 dye had a υ_2 of 0.688 for a 940 nm layer thickness, suggesting an increased pore filling by the organic fraction even though this layer is thicker than the other two mixed samples. From prior literature on this subject, reduced filling with increased layer thickness is expected.[8,9] Our SEM/EDX analysis also shows reduced filling with increased layer thickness (Fig. 9). These two pieces of data together point to better filling with the Z907 dye-coated TiO_2. However, we did not conduct a systematic study of pore filling using ellipsometry on samples with known filling. It is for this reason that we believe that the result, while interesting, is still within the error of the measurement. Literature estimates of pore volume are 59% to 71%.[18] These results indicate that for thin films, the pores are >90% filled.

D. SEM/EDX

It has been shown that one of the major restrictions on the thickness of SDSC devices is the difficulty in filling the porous matrix of TiO_2 with an organic hole conductor.[8] Numerous different hole conductors have been tested for use in SDSC devices, but spiro-MeOTAD has been shown to make by far the most efficient devices because it is able to wet the surface of the dye-covered TiO_2 without forming crystalline domains.[11] It is assumed that since the spiro-MeOTAD does not crystallize, it prefers to stick to the porous TiO_2 structure rather than to itself.

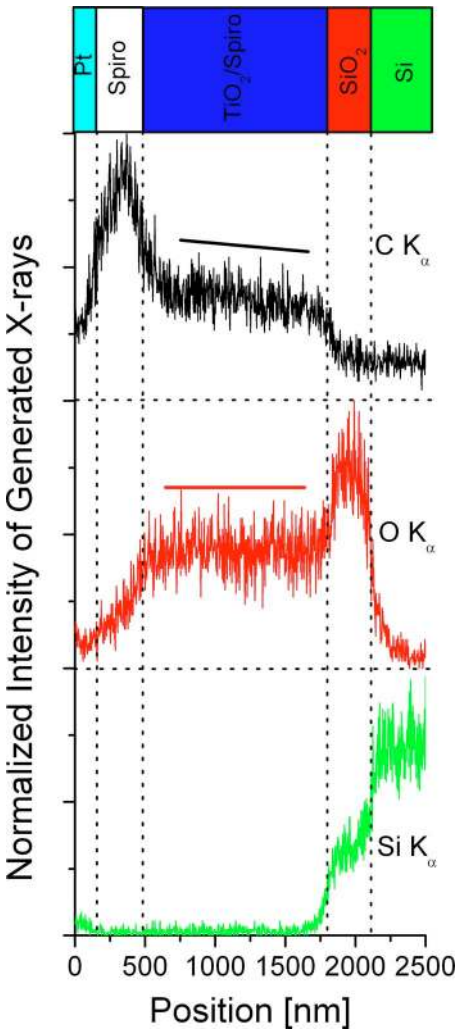

FIG. 9. (Color online) SEM-EDX of carbon (black), oxygen (red), and silicon (green) for a porous TiO_2 layer filled with spiro-MeOTAD on a $Si-SiO_2$ substrate that has had Pt sputtered on top. The substrate was polished prior to imaging. The relative thicknesses of the various layer is shown by a schematic and vertical dotted lines. A linear fit to the carbon signal in the active layer shows decreasing filling while the oxygen signal is constant.

In this article we measured the optical parameters of the layers used in a SDSC. We showed in Fig. 5 that the unfilled TiO_2 matrix scatters light and makes ellipsometric analysis impossible. The ellipsometry was therefore performed on mesoporous TiO_2 that was filled with spiro-MeOTAD. To confirm that the layers were completely filled, the films were broken and then SEM-EDX was performed on the cross section (Fig. 9). This technique was performed on Ar ion-polished cross sections of the presented ellipsometry samples at low electron acceleration voltages in order to avoid artificial x-ray signals. SEM-EDX allows an elemental mapping of the prepared surface as a function of position with a resolution of ~100 nm at the applied acceleration voltage.

Figure 9 shows line scans of EDX signal versus position perpendicular to the cross section of a filled layer with an active layer thickness of ~1300 nm for the elements C, O, and Si. A cartoon of the layer structure and dotted lines are included. The C signal is highest in the spiro-MeOTAD (as expected), drops down a little at the transition to the mixed layer, decreases throughout the mixed layer, and drops down to roughly zero at the transition to the SiO_2. The O signal is essentially flat in the mixed layer and higher in the SiO_2 layer. The Si signal is zero in the mixed layer and shows increases in the SiO_2 and Si layers as expected.

The interpretation of the data (Fig. 9) is that the spiro-MeOTAD has reduced penetration into the porous TiO_2 with increased depth into the mixed layer where the O signal is constant. The C signal appears to decrease throughout the active layer with lesser filling at greater depth into the porous TiO_2. The small drop in the carbon signal at the transition between mixed and SiO_2 layers verifies that the deep pores are at least partially filled. This data shows conclusively that increased thickness of the porous TiO_2 layer leads to reduced pore filling of the spiro-MeOTAD. We used samples with mixed layers that were very thin, <900 nm for all ellipsometry measurements in order to ensure adequate pore filling throughout the layer thickness. Use of these thin layers allows high quality optical data to be obtained using ellipsometry, whereby layers with normal device thicknesses (~2 μm) cannot yield accurate optical data. A detailed analysis of the pattern of pore filling as functions of layer thickness and of the SEM-EDX techniques used can be found elsewhere.[32]

IV. CONCLUSIONS

In conclusion, we have developed methods to measure the complex refractive index for all of the layers in a SDSC. Each of the layers was independently measured using spectroscopic ellipsometry and fit by reducing the MSE to the measured data with the simplest optical model possible. The problem of the fitting procedure finding an incorrect local minima in the parameter space was eliminated by comparing measured transmission spectra on quartz substrates to calculated absorbance spectra using the $n(\lambda)$ and $k(\lambda)$ from ellipsometry and layer thicknesses obtained from profilometry and SEM imaging. The optical parameters are suitable for multilayer optical modeling of complete SDSC devices as long as the assumptions inherent in the measurement technique are carried over to the device models. These assumptions are (1) that the spiro-MeOTAD completely fills the TiO_2 matrix, which means that scattering is neglected from void pockets, (2) that the roughness of the mixed layer/spiro-MeOTAD interface can be neglected, again that scattering is neglected, and (3) that all of the layers are prepared according to the fabrication methods outlined here.

We acknowledge the Alexander von Humboldt foundation for the postdoctoral grant of AM. We also thank the Ministry of Science and Innovation of Northrhine-Westfalia (EleNa-project) and the United States Department of Energy under Grant No. DE-FG3608GO18018.

[1] B. O' Regan and M. Grätzel, Nature (London) **353**, 737 (1991).
[2] M. Grätzel, Chem. Lett. **34**, 8 (2005).
[3] U. Bach, D. Lupo, P. Comte, J. E. Moser, F. Weissörtel, J. Salbeck, H. Spreitzer, and M. Grätzel, Nature (London) **395**, 583 (1998).
[4] H. J. Snaith, A. Moule, C. Klein, K. Meerholz, R. H. Friend, and M. Grätzel, Nano Lett. **7**, 3372 (2007).
[5] S. Ito, S. M. Zakeeruddin, R. Humphry-Baker, P. Liska, R. Charvet, P. Comte, M. K. Nazeeruddin, P. Pechy, M. Takata, H. Miura, S. Uchida, and M. Grätzel, Adv. Mater. **18**, 1202 (2006).

[6]A. Hagfeldt and M. Grätzel, Acc. Chem. Res. **33**, 269 (2000).
[7]L. Schmidt-Mende, S. M. Zakeeruddin, and M. Grätzel, Appl. Phys. Lett. **86**, 013504 (2005).
[8]L. Schmidt-Mende and M. Grätzel, Thin Solid Films **500**, 296 (2006).
[9]H. J. Snaith, R. Humphry-Baker, I. Cesar, S. M. Zakeeruddin, and M. Grätzel, Nanotechnology **19**, 424003 (2008).
[10]J. Kruger, R. Plass, M. Grätzel, P. J. Cameron, and L. M. Peter, J. Phys. Chem. B **107**, 7536 (2003).
[11]J. E. Kroeze, N. Hirata, L. Schmidt-Mende, C. Orizu, S. D. Ogier, K. Carr, M. Grätzel, and J. R. Durrant, Adv. Funct. Mater. **16**, 1832 (2006).
[12]U. Bach, Y. Tachibana, J. E. Moser, S. A. Haque, J. R. Durrant, M. Grätzel, and D. R. Klug, J. Am. Chem. Soc. **121**, 7445 (1999).
[13]D. M. Huang, H. J. Snaith, M. Grätzel, K. Meerholz, and A. J. Moulé, J. Appl. Phys. 106, 073112 (2009).
[14]S. Adachi, Phys. Rev. B **38**, 12966 (1988).
[15]Schott Glass Inc., Online Publications (2008).
[16]L. Kavan and M. Grätzel, Electrochim. Acta **40**, 643 (1995).
[17]H. J. Snaith and M. Grätzel, Adv. Mater. **18**, 1910 (2006).
[18]C. J. Barbé, F. Arendse, P. Comte, M. Jirousek, F. Lenzmann, V. Shklover, and M. Grätzel, J. Am. Ceram. Soc. **80**, 3157 (1997).
[19]P. Wang, S. M. Zakeeruddin, J. E. Moser, M. K. Nazeeruddin, T. Sekiguchi, and M. Grätzel, Nature Mater. **2**, 402 (2003).
[20]T. Horiuchi, H. Miura, K. Sumioka, and S. Uchida, J. Am. Chem. Soc. **126**, 12218 (2004).
[21]H. J. Snaith and M. Grätzel, Appl. Phys. Lett. **89**, 262114 (2006).
[22]H. Takahashi, A. Sato, M. Takakura, N. Mori, J. Boerder, W. Knoll, and J. Critchell, Mikrochim. Acta **155**, 295 (2006).
[23]H. G. Tompkins and W. A. McGahan, *Spectroscopic Ellipsometry and Reflectometry* (Wiley, New York, 1999).
[24]N. K. Persson, M. Sun, P. Kjellberg, T. Pullerits, and O. Inganas, J. Chem. Phys. **123**, 204718 (2005).
[25]E. D. Palik, *Handbook of Optical Constants of Solids* (Academic, San Diego, 1985), Vol. 1.
[26]L. A. A. Pettersson, L. S. Roman, and O. Inganas, J. Appl. Phys. **86**, 487 (1999).
[27]P. Peumans, A. Yakimov, and S. R. Forrest, J. Appl. Phys. **93**, 3693 (2003).
[28]A. J. Moulé and K. Meerholz, Appl. Phys. B: Lasers Opt. **86**, 721 (2007).
[29]E. Hecht, *Optics*, 4th ed. (Pearson Education, Inc., San Francisco, 2002).
[30]L. K. H. Beek, *Progress in Dielectrics*, Dielectric Behaviour of Heterogeneous Systems, Vol. 7 (Heywood Books, London, 1967).
[31]G. E. Jellison and F. A. Modine, Appl. Phys. Lett. **69**, 371 (1996).
[32]I.-K. Ding, N. Tetreault, J. Brillet, B. E.Hardin, E. H. Smith, S. J. Rosenthal, F. Sauvage, M. Grätzel, and M. D. McGehee, Adv. Funct. Mater. **19**, 1 (2009).